LLNL-JRNL-2014952

Lawrence Livermore National Laboratory

# High-Power Impulse Magnetron Sputter Deposition of Boron Carbide with Full-Face Erosion Magnetron and Mixed Ar-Ne Plasma

G Taylor

January 2026

Fusion Science and Technology

## Disclaimer



This work performed under the auspices of the U.S. Department of Energy by Lawrence Livermore National Laboratory under Contract DE-AC52-07NA27344.

Fusion Science and Technology

# High-power impulse magnetron sputter deposition of boron carbide with full-face erosion magnetron and mixed Ar-Ne plasma

--Manuscript Draft--

| | |
|---|---|
| **Manuscript Number:** | FST24-266R1 |
| **Full Title:** | High-power impulse magnetron sputter deposition of boron carbide with full-face erosion magnetron and mixed Ar-Ne plasma |
| **Article Type:** | Research Article |
| **Keywords:** | Ablator capsule; high-power impulse magnetron sputtering; oblique angle deposition |
| **Manuscript Classifications:** | 14: 14 Materials and radiation effects; 16: 16 Power conversion; 23: 23 Fabrication, assembly, and maintenance; 27: 27 Advanced manufacturing techniques; 29: 29 Inertial fusion engineering |
| **Corresponding Author:** | Gregory Taylor<br>Lawrence Livermore National Laboratory<br>UNITED STATES |
| **Corresponding Author Secondary Information:** | |
| **Corresponding Author's Institution:** | Lawrence Livermore National Laboratory |
| **Corresponding Author E-Mail:** | taylor6q@comcast.net |
| **Corresponding Author's Secondary Institution:** | |
| **First Author:** | Gregory Taylor |
| **First Author Secondary Information:** | |
| **Order of Authors:** | Gregory Taylor |
| | Samarra Graiser |
| | Leonardus-Bimo Bayu Aji |
| | Swanee Shin |
| | Daniel Goodelman |
| | Xavier Lepro Chavez |
| | Sergei Kucheyev |
| **Order of Authors Secondary Information:** | |
| **Manuscript Region of Origin:** | UNITED STATES |
| **Abstract:** | Boron carbide (B4C) is an attractive inertial confinement fusion ablator material. The fabrication of B4C ablators by magnetron sputtering requires process optimization. To increase process flexibility, here, we explore high-power impulse magnetron sputter (HiPIMS) deposition of B4C in pure Ar and mixed Ar-Ne plasmas. Results show that higher plasma discharge currents can be reached with a mixed Ar-Ne plasma in the entire working pressure range studied (5 − 50 mTorr). At 45 mTorr with 10% of Ne in the Ar-Ne mix, high peak target current densities of ~ 1 A cm−2 are demonstrated. Films deposited with such a mixed Ar-Ne plasma with a full-face erosion magnetron source on substrates biased at −25 V exhibit higher density and improved mechanical properties albeit with higher compressive residual stresses compared to the case of HiPIMS deposition in a pure Ar plasma. This work demonstrates additional process flexibility of the HiPIMS discharge mode for the deposition of B4C coatings. |
| **Author Comments:** | Thank you for your consideration. |

August 1, 2025

Ref: **FST24-266**
247741373
High-power impulse magnetron sputter deposition of boron carbide with full-face erosion magnetron and mixed Ar-Ne plasma
by Gregory Taylor et al.

**Point-by-point response to reviewers' comments**

We thank the reviewers for appreciating our work and providing constructive feedback aimed at improving the clarity and quality of this manuscript. Below is our detailed, point-by-point response, indicating where changes have been made in the revised manuscript. A marked version of the manuscript highlighting the changes is also included in this resubmission.

**Response to comments of Reviewer 1**

--- Reviewer 1, comment 1

Authors indicated ultimate goal is to coat on spherical mandrels. What is the implication the data presented will have on the coating on spheres.

--- Response to Reviewer 1, comment 1

Deposition on spheres is inherently an oblique angle deposition process, meaning that the growth processes are not only determined by particle energies, adatom mobility, and absorption probabilities, but also by "shadowing effects" and ballistic momentum transfer effects. Shadowing involves the prevention of incident particles from arriving at areas shadowed in the line of sight of depositing species flux. The custom-designed faceted substrate holder used in the present study enables us to systemically observe and measure effects of oblique angle deposition on microstructure major film properties at various substrate tilt angles.

This study demonstrates that the reduction in mechanical properties and densities of coatings deposited at oblique angles can be mitigated via HiPIMS with a mixed Ar/Ne plasma. For ICF ablator coatings on spheres, these improvements at oblique angles have major implications because having a dense and mechanically robust capsule increases its chance of survivability during various handling and processing steps that the capsule undergoes during target fabrication.

We have clarified some of these points on P. 3 of the revised manuscript.

--- Reviewer 1, comment 2

It is noted that under heated substrate the base pressure achieved is 4x10-6 torr. With this elevated background pressure, what is the impact to the coating quality, stress and density etc.

--- Response to Reviewer 1, comment 2

While the effect of base pressure during B4C sputter deposition has not been studied systemically as of yet, our recent study (Ref. 14 of the revised manuscript) has explored a wider set of base pressure conditions of (5-200) x 1e-7 Torr to shine some light on effects of residual chamber gas. In this previous study (Ref. 14), it was observed that O-content in resultant films was low (< 1 at.%), below the amount detected in the starting B4C sputtering target itself (~2.5 at.% O). These observations of low levels of oxygen incorporation have been attributed to the volatility of oxygen-containing species that could form from B, C, H, and O interactions in vacuum during the deposition process. In other words, this previous study (Ref. 14) suggests negligible effects of the elevated pressure of residual gases in the chamber (in the range studied) on the deposition process.

We clarify these points on P. 3 of the revised manuscript.

--- Reviewer 1, comment 3

Very high gas pressure is used for HiPIMS coating, e.g. 45mTorr. What is the high pressure contribution to coating stress, density etc.

--- Response to Reviewer 1, comment 3

Elevated working pressure is expected to increase vapor phase scattering of sputtered particles, leading to the thermalization of depositing species flux and to a broadening of the distribution of particle impact angles. As a result, films deposited at higher working gas pressures are expected to have lower residual compressive stress and reduced adhesion. We clarify it on P. 4 of the revised manuscript.

--- Reviewer 1, comment 4

Since Ar ionization energy is 15.7ev and Ne ionization energy is 21.5eV. Ne is harder to ionize than Ar. Can authors explain why mixing Ne will enhance ionization.

--- Response to Reviewer 1, comment 4

The addition of Ne to a predominantly Ar plasma modifies plasma properties in non-trivial ways. The ionization potential of Ne is indeed significantly larger than that of Ar. However, Ne also has much higher electron impact ionization cross section, and Ne ion bombardment of the B4C target

emits more secondary electrons that act as the main “fuel” for the magnetron discharge. Several previous studies (see, for example, Refs. 22-23 of the revised manuscript) have clearly demonstrated that the addition of Ne to the predominantly Ar plasma leads to an increased electron temperature and, hence, a higher fraction of the ionized atoms in depositing species flux. We clarify these points on P. 3 of the revised manuscript and add Refs. 22-23.

**Response to comments of Reviewer 3**

--- Reviewer 3, comment 1

The x-axis in figure 3 is inconsistent between a-d and e, leaving a-d unlabeled. The axis should be adjusted for consistency across all graphs a-e.

--- Response to Reviewer 3, comment 1

The plot has been corrected. Thank you.

--- Reviewer 3, comment 2

Dep. Rate and density data are missing in Figure 3 for high tilt angle depositions, though other film properties are included. This should be addressed in the discussion, particularly as the stress, hardness, and Young's Modulus change significantly for tilt angle = 90.

--- Response to Reviewer 3, comment 2

The missing deposition rate data has been included for the 90° substrate tilt angles.

--- Reviewer 3, comment 3

The authors should consider adding discussion of the relationship between the deposition rate and the film density. Typically, one might expect the normalized deposition rate to decrease as film density increases. That this is not observed in this work suggests the sputter rate may be increasing significantly upon adding Ne.

--- Response to Reviewer 3, comment 3

In Fig. 3(e) of the revised manuscript, we have added the missing data point at 80°. With the measurement method of this study (i.e., RBS), density could be measured only for films deposited

on substrates with a tantalum marker layer. In the revised manuscript, we clarify that Ta-coated substrates could only be placed on 0-80 degree facets.

On P. 7 of the revised manuscript, we discuss the relationship between deposition rate and film density. The fact that the deposition rate does not decrease with increasing film density indeed suggests that the addition of Ne results in an increase in the sputter rate of the target.

--- Reviewer 3, comment 4

Previous studies of B4C deposition by DCMS and HiPIMS (e.g. https://doi.org/10.1007/s10853-016-0262-4) found the film composition was sensitive to process pressure. The changes in film properties observed by the authors may be attributable to a change in the stoichiometry of the deposited films. The authors should consider adding discussion of their expected film composition and how it might be impacted by introducing Ne and by the change in substrate angle.

--- Response to Reviewer 3, comment 4

In the present study, we did not measure the stoichiometry of B4C films since these films were too thin for RBS measurements so that the signal from the Si substrate was interfering with signals from B, C and O. Film stoichiometry, however, was measured in several of our previous studies of sputter deposited B4C (Refs. 12-18 of the revised manuscript). These previous studies have revealed that the B/C ratio in films was the same as the B/C ratio in the starting sputtering target, as expected from negligible volatility of B and C at these temperatures and similar masses and, hence, angular emission profiles of sputtered B and C atoms.

**Revision #1 of FST24-266**

# High-power impulse magnetron sputter deposition of boron carbide with full-face erosion magnetron and mixed Ar-Ne plasma

G. V. Taylor, S. Graiser, L. B. Bayu Aji, S. J. Shin, D. C. Goodelman, X. Lepro Chavez, and S. O. Kucheyev

*Lawrence Livermore National Laboratory, Livermore, California 94550, U.S.A.*

(Dated: 2 August 2025)

Boron carbide ($B_4C$) is an attractive inertial confinement fusion ablator material. The fabrication of $B_4C$ ablators by magnetron sputtering requires process optimization. To increase process flexibility, here, we explore high-power impulse magnetron sputter (HiPIMS) deposition of $B_4C$ in pure Ar and mixed Ar-Ne plasmas. Results show that higher plasma discharge currents can be reached with a mixed Ar-Ne plasma in the entire working pressure range studied ($5-50$ mTorr). At 45 mTorr with 10% of Ne in the Ar-Ne mix, high peak target current densities of $\sim 1$ A cm$^{-2}$ are demonstrated. Films deposited with such a mixed Ar-Ne plasma with a full face erosion magnetron source on substrates biased at $-25$ V exhibit higher density and improved mechanical properties albeit with higher compressive residual stresses compared to the case of HiPIMS deposition in a pure Ar plasma. This work demonstrates additional process flexibility of the HiPIMS discharge mode for the deposition of $B_4C$ coatings.

## I. INTRODUCTION

The widespread use of boron carbide ($B_4C$) for nuclear, defense, aerospace, and tribological applications is owed to its distinct set of properties.[1] Low density in combination with high mechanical strength, hardness, and chemical stability make $B_4C$ an excellent material for ballistic armor plating[2] and various wear-resistant coatings.[3] In addition, the high neutron absorption cross-section and excellent thermal and mechanical properties make $B_4C$ attractive for nuclear reactor applications, including reaction control rods, neutron detectors, and radiation shielding.[4,5] Moreover, $B_4C$ is an attractive next-generation ablator material for inertial confinement fusion (ICF) and inertial fusion energy (IFE) applications.[6,7] For ICF and IFE, $B_4C$ is required in the form of hollow spherical shells with a diameter of $\sim 0.5 - 5.0$ mm and a wall thickness of $\sim 20 - 200$ $\mu$m.[8]

Magnetron sputtering[9] is currently the leading method for the fabrication of such spherical $B_4C$ shells for ICF and IFE.[8,10,11] It is a highly repeatable and scalable physical vapor deposition technique with a large and tunable parameter space.[9] It is used in many industries to deposit both metals and ceramics. Recent developments in magnetron sputtering of $B_4C$ include systematic studies of working gas pressure,[12,13] substrate temperature,[8,14] substrate tilt angles,[8,13,15–17] and plasma composition[15,18] on film properties. A significant reduction in the density of nodular defects has been demonstrated for $B_4C$ films deposited with a full face erosion (FFE) magnetron source.[17] A follow up work[11] has explored the FFE source deposition of $B_4C$ onto rolling spherical substrates, as required for ICF ablator capsule fabrication. All these previous studies[8,11–18] have used either the direct current magnetron sputtering (DCMS) or radio-frequency magnetron sputtering (RFMS) plasma discharge mode.

High-power impulse magnetron sputtering (HiPIMS)[19,20] is another plasma discharge mode offering expanded process flexibility compared to conventional DCMS and RFMS modes. Schmidt *et al.*[21] have evaluated HiPIMS deposition of $B_4C$, with the focus on effects of Ar working gas pressure at two substrate temperatures of 100 and 400 °C. They have compared films deposited by DCMS and HiPIMS discharge modes, with relatively low peak target current densities of $\sim 0.16$ A cm$^{-2}$. They found a negligible difference in properties of films deposited onto electrically floating substrates by DCMS or HiPIMS. Their results suggest that, for such low peak target current densities and their specific

experimental conditions, HiPIMS adds process complexity but offers no advantage over conventional DCMS.

Here, we explore the capabilities of HiPIMS deposition of $B_4C$ by capitalizing on our recent findings of reduced nodular defect densities in films deposited with FFE magnetrons[17] and higher discharge current densities for Ne-containing plasmas.[18] The addition of Ne to a predominantly Ar plasma has also been demonstrated to increase electron temperature and, hence, the degree of ionization of of depositing species flux.[22,23] We use an FFE magnetron source operated in the HiPIMS mode and compare properties of films deposited on negatively biased substrates with different tilt angles in pure Ar and mixed Ar-Ne plasmas with peak target current densities of $\sim 1$ A cm$^{-2}$. The understanding of oblique angle deposition effects is directly relevant to ICF and IFE ablator fabrication since it involves the deposition onto non-planar (spherical) substrates.[8] Our results demonstrate that HiPIMS offers additional process flexibility for $B_4C$ deposition and warrants further systematic studies.

## II. METHODS

Table I summarizes deposition conditions for the two coating runs of the present study. Coatings were deposited in a cylindrical high-vacuum chamber with a diameter and height of 44 and 36 cm, respectively. Prior to admitting working gases into the chamber, the substrate holder was heated to 450 °C, corresponding to a substrate temperature of 330 °C, and the chamber pressure was $\sim 5 \times 10^{-6}$ Torr. Our previous study[14] has found negligible effects of the residual chamber pressure, in the range of $(5 - 200) \times 10^{-7}$ Torr, on the elemental composition of sputter deposited $B_4C$ films. Depositions were performed with a 75-mm diameter circular FFE magnetron source (Gencoa Ltd, model FFE-75, UK) modified for direct target cooling. The source axis was positioned horizontally. Disk-shaped $B_4C$ targets (Feldco International, USA) had a diameter of 71 mm, an initial thickness of 3 mm, a density of 2.4 g cm$^3$ and an electrical resistivity of $\sim 2 \times 10^4$ Ω cm. Disks of $B_4C$ were bonded with In to 2-mm-thick Mo backing plates. The total thickness of the bonded target assembly at the thinnest point of the racetrack before and after each deposition experiment was in the range of $4.84 - 4.91$ mm. The DC plasma was driven with an Advanced Energy MDX 1K power supply unit. The HiPIMS plasma was driven with an Advanced Energy MDX 1K power supply unit, which was coupled to a high-voltage pulser unit (Ionautics, model

HiSPTER 1, Sweden). The two deposition runs described here were done in the constant peak target voltage mode.

Depositions were performed with high purity Ar (99.998 %) and Ne (99.998 %) gases. Following a survey of various partial pressures of Ne, we used an Ar-Ne mix with 10% of Ne and a long pulse duration as it resulted in a stable plasma discharge at 45 mTorr. Such a relatively high working gas pressure of 45 mTorr was also chosen to minimize compressive residual stress in films, based on our previous study.[12] The total working gas flow rate was 55 standard cubic centimeters per minute. Prior to each run, a 30-minute pre-conditioning of the target was performed at the set point parameters with the substrates shielded from the target by an electrically grounded shutter.

Substrates were mounted on a custom-designed faceted substrate holder machined from a solid Mo block, which was described previously.[16] Heating of the substrate holder was achieved with an electrically grounded resistive heater (HeatWave Labs Inc., model 112868, USA). Substrates were mechanically clamped to the holder with Mo screws and washers. In this configuration, the normal of substrate holder facets were at the following angles ($\alpha$) to the magnetron source axis: 0°, 20°, 40°, 60°, 80°, and 90°. The two substrate types used were (i) $10 \times 10$ mm$^2$ Si (100) chips with a 200-nm-thick Ta metal layer deposited on top in a separate DCMS run used for density measurements and (ii) $3 \times 12$ mm$^2$, 280 $\mu$m thick Si (100) cantilevers used for residual stress, mechanical properties, and deposition rate measurements. Due to design restrictions of the faceted substrate holder, chips were only included on facets with $\alpha = 0 - 80°$, while cantilevers were placed on all six facets. To ensure consistent initial substrate cleanliness, we used the following three-step substrate cleaning procedure in an ultrasonic bath (with 15 minutes for each step): (i) acetone, (ii) ethanol, and (iii) a water-based detergent solution. This was followed by a final rinse in de-ionized water and blow drying with dry nitrogen.

Film thickness was measured by stylus profilometry (Bruker, model Dektak XT, USA). Residual stress in films was calculated with the Stoney equation based on the change in cantilever curvature measured by profilometry before and after deposition. The thermal stress component originating from the difference in coefficients of thermal expansion between the $B_4C$ film and Si substrate was estimated to be 100 MPa (tensile), as in our previous studies.[16,17] The Ta layer on Si chips was used as a marker in the areal density measurements by Rutherford backscattering spectrometry (RBS) with a 2 MeV $^1H^+$ ion

beam. The presence of this Ta marker layer has a negligible effect on the properties and morphology of $B_4C$ films deposited as substrate temperatures of the present study.[8]

Mechanical properties were evaluated by nanoindentation (MTS, model XP, USA) in the load-controlled mode with a Berkovich diamond tip. Meyer's hardness ($H_M$) was defined as average contact pressure, and Young's Modulus ($E_Y$) was calculated based on the conventional Oliver-Pharr method.[24] In Oliver-Pharr calculations, we assumed Poisson's ratios of diamond and $B_4C$ films of 0.07 and 0.17, respectively, and Young's modulus of diamond of 1141 GPa.[25] Values of $H_M$ and $E_Y$ were averaged over the indenter penetration depth range of $\sim 10 - 20\%$ of film thickness.

## III. RESULTS AND DISCUSSION

### A. Discharge characteristics

Figure 1 shows dependencies of DCMS plasma discharge target current ($I_t$) versus target voltage ($V_t$) for Ar-Ne mixes with 0 and 10% of Ne, collected at three representative working pressures. In the entire pressure range studied of $5 - 50$ mTorr, for both gas mixes, the discharge behavior is qualitatively similar. All $I_t(V_t)$ curves are superlinear, as commonly observed for Ar magnetron discharges[9] and different from the abnormal $I_t(V_t)$ dependence characteristic of the discharge with a pure Ne plasma.[18]

As working pressure is increased, Fig. 1 shows that $I_t$ at any given $V_t$ increases. Hence, higher $I_t$ values at lower voltages can be achieved at larger working pressures. While this general trend is the same for Ar-Ne mixes with 0 and 10% of Ne, the effect of pressure on the $I_t(V_t)$ dependence is significantly larger for the 10% Ne case. This could be attributed to a combination of (i) a reduction in rarefaction[26] near the target surface due to the higher thermal conductivity and smaller collisional cross section of Ne compared to Ar and (ii) a higher secondary ion-electron emission coefficient of Ne.[18,27] It is seen from Fig. 1 that, for a given $V_t$, larger $I_t$ is achieved for higher pressure with 10% of Ne in the mix. Hence, we chose these conditions for HiPIMS film deposition runs of the present study (Table I).

Figure 2 shows waveforms of $I_t$ [Fig. 2(a)] and substrate current [$I_s$, Fig. 2(b)] for Ar-Ne mixtures with 0 and 10% of Ne with at 45 mTorr. For both working gas configurations, the HiPIMS waveforms have peak target currents that are two-orders of magnitude greater than

their DCMS counterparts at similar average discharge power (Fig. 1). It is also seen from Fig. 2(a) that the admix of Ne to the plasma helps achieve higher peak currents. The peak $I_t$ and $I_s$ for the 10% of Ne mix are $\sim 2$ times those for the 0% Ne case, leading to a higher plasma density and larger flux of ions bombarding the film surface during growth with the Ne-containing plasma.

The shape of $V_t$ and $V_s$ waveforms in Figs. 2(a) and 2(b) are qualitatively the same. They exhibit a gradual increase to a peak at $\sim 150$ $\mu$s from the pulse start, followed by a decrease and saturation for $\gtrsim 400$ $\mu$s. This waveform shape is qualitatively similar to those revealed in our recent systematic study of HiPIMS deposition of Au-Ta alloys with 2-inch MAK-model magnetron sources.[28] However, the time scales are $\sim 4$ times slower for the $B_4C$ discharge. This is an interesting observation with practical implications for deposition process optimization, and more work is clearly needed to better understand $B_4C$ HiPIMS plasma and deposition processes.

## B. Film properties

Figure 3(a) shows the substrate tilt angle ($\alpha$) dependence of the deposition rate. The rate has been normalized by the average discharge power in order to compare results for two runs with 0 and 10% of Ne in the Ar-Ne mix performed at constant peak target voltage and different peak $I_t$ and average discharge power values (Table I). It is seen from Fig. 3(a) that, for both cases of 0 and 10% of Ne, the deposition rates are essentially identical. Interestingly, the rapid decrease in the deposition rate with increasing $\alpha$ observed in several previous investigations[13,16–18] of DCMS and RFMS deposition of $B_4C$ is not seen in Fig. 3(a). Instead, a decrease in the deposition rate occurs between $\alpha = 0°$ and 20°, followed by a nearly constant rate for $\alpha$ in the range of $20 - 60°$, and then another decrease for strongly oblique angles of $\alpha = 80$ and 90°. This observation may result from a combination of high working pressure of 45 mTorr, resulting in efficient scattering of depositing species flux, and ion extraction through the substrate plasma sheath due to the electric field generated from the negative substrate bias. A follow up systematic investigation of depositing species flux as well their energy and angular distributions could help better understand this unexpected behavior.

Figure 3(b) shows the $\alpha$ dependence of residual stress ($\sigma$), revealing that, compared to

the case of pure Ar plasma deposition, films deposited with a 10% Ne mix have higher compressive $\sigma$ for low $\alpha$ cases of 0 and 20°. For example, for untilted films, compressive $\sigma$ increases from 1.4 to 2.2 GPa with the addition of Ne to the plasma. This can be attributed to a corresponding increase in ion flux [Fig. 2(b)]. For both plasma conditions, $\sigma$ is close to zero for $\alpha$ of 40° and above. This suggests that the growth of films at such oblique angles is dominated by oblique angle atomic impacts resulting in a columnar microstructure with low residual stress.[16]

As shown in Fig. 3(c), high hardness values ($H_M$ = 38 GPa) are measured in coatings from both runs for the $\alpha = 0°$ tilt angle. For larger $\alpha$ films, $H_M$ values for 0 and 10% of Ne cases diverge. Films deposited with 10% of Ne have consistently higher $H_M$ values. The same trend is replicated by the $\alpha$ dependence of $E_Y$ shown in Fig. 3(d). Films deposited with a 10% of Ne are stiffer. This trend could be explained by examining the evolution of film density shown in Fig. 3(e). It reveals that films deposited with the Ne-containing plasma have higher density although their their normalized deposition rates are largely the same [Fig. 3(a)]. This suggests that the deposition with a Ne-containing plasma is characterized by an increased target sputtering rate. Films deposited with a 100% Ar plasma have a density of 2.4 g/cm$^3$ at $\alpha = 0°$, $\sim$ 2.0 g/cm$^3$ for $\alpha$ in the range of $0 - 60°$, and 1.8 g/cm$^{-3}$ for $\alpha = 80°$. Films deposited with a 10% Ne mix exhibit a similar trend but with overall higher density values. Overall, the density in films is shown to be weakly dependent on substrate tilt angle, and this is especially the case for the 10% Ne samples. This behavior could be attributed to a larger ion-to-atom fraction and more efficient ion bombardment of the growing film surface for the case of Ne-containing plasma although additional systematic studies involving plasma diagnostics are currently needed to better understand film growth mechanisms and optimize the deposition process.

## IV. SUMMARY

We have used magnetron sputtering to deposit $B_4C$ films with an FFE source modified for direct cooling with the HiPIMS plasma discharge mode with two different working gases (pure Ar and an Ar-Ne mix with 10% of Ne) and substrates biased at $-25$ V. Higher plasma densities, as indicated by larger target and substrate currents, can be achieved by using larger process pressure and adding Ne to the working gas mixture. This work has

demonstrated that the density and mechanical properties of $B_4C$ films can be improved with the deposition in the HiPIMS mode in an Ar-Ne working gas mix. Our results demonstrate that the HiPIMS discharge mode coupled with Ar-Ne gas mixture expands the flexibility of magnetron sputter deposition of $B_4C$ and offers additional process control. However, it also increases process complexity, and more work is currently needed to better understand the physics of the HiPIMS $B_4C$ mixed plasma discharge with an FFE magnetron source.

## V. ACKNOWLEDGMENTS

This work was performed under the auspices of the U.S. DOE by LLNL under Contract DE-AC52-07NA27344.

## VI. DATA AVAILABILITY STATEMENT

The data that supports the findings of this study is available within the article.

## VII. AUTHOR DECLARATIONS

### A. Conflict of Interest

The authors have no conflicts to disclose.

## REFERENCES


[1]F. Thévenot, "Boron carbide—A comprehensive review," *Journal of the European Ceramic Society*, vol. 6, no. 4, pp. 205, 1990.

[2]S. G. Savio, et al., "An experimental study on ballistic performance of boron carbide tiles," *International Journal of Impact Engineering*, vol. 38, no. 7, pp. 535, 2011.

[3]S. Bhatia, et al., "A review on mechanical and tribological characterization of boron carbide reinforced epoxy composite," *Advanced Composite Materials*, vol. 30, no. 4, pp. 307, Taylor & Francis, 2021.

[4]B. S. Gajjar, et al., "Boron Carbide as High-Energy Radiation Shielding Material for ITER," *IEEE Transactions on Plasma Science*, vol. 50, no. 12, pp. 5078, 2022.

[5]Y. Q. Chen and B. H. Yan, "The technology of shielding design for nuclear reactor: A review," *Progress in Nuclear Energy*, vol. 161, 104741, 2023.

[6]S. W. Haan, et al., "Design and modeling of ignition targets for the National Ignition Facility," Physics of Plasmas, vol. 2, no. 6, pp. 2480, 1995.

[7]T. R. Dittrich, S. W. Haan, S. Pollaine, A. K. Burnham, and G. L. Strobel, "NIF capsule design update," Fusion Sci. Tech. **31**, 402 (1997).

[8]S. O. Kucheyev, et al., "Development of New Magnetron Sputter Deposition Processes for Laser Target Fabrication," *Fusion Science and Technology*, vol. 79, no. 7, pp. 823, American Nuclear Society, 2023.

[9]W. D. Westwood, Sputter deposition, AVS, New York (2003).

[10]A. K. Burnham, C. S. Alford, D. M. Makowiecki, T. R. Dittrich, R. J. Wallace, E. C. Honea, and C. M. King, "Evaluation of B4C as an Ablator Material for NIF Capsules," Fusion Sci. Tech. **31**, 456 (1997).

[11]J. B. Merlo, et al., "Magnetron sputter deposition of ultrathick boron carbide coatings on spherical substrates for inertial confinement fusion," *Surface and Coatings Technology*, vol. 477, 130321, 2024.130321.

[12]A. M. Engwall, L. B. Bayu Aji, S. Shin, P. B. Mirkarimi, J. H. Bae, and S. O. Kucheyev, J. Appl. Phys. **128**, 175301 (2020).

[13]L. B. Bayu Aji, et al., "Radio-frequency magnetron sputter deposition of ultrathick boron carbide films," *Journal of Vacuum Science & Technology A*, vol. 41, no. 2, 023407, 2023.

[14]L. B. Bayu Aji, et al., "Effect of substrate temperature on sputter-deposited boron carbide films," *Journal of Applied Physics*, vol. 131, no. 7, 075304, 2022.

[15]S. J. Shin, L. B. Bayu Aji, A. M. Engwall, J. H. Bae, G. V. Taylor, P. B. Mirkarimi, C. Aracne-Ruddle, J. Nguyen, C. W. N. Kong, and S. O. Kucheyev, Fusion Sci. Technol. **79**, 841 (2023).

[16]S. J. Shin, et al., "Oblique angle deposition of boron carbide films by magnetron sputtering," *Journal of Applied Physics*, vol. 130, no. 12, 125305, 2021.

[17]G. V. Taylor, et al., "Boron carbide films with reduced nodular defect density deposited by full-face erosion radio-frequency magnetron sputtering," *Journal of Vacuum Science & Technology A*, vol. 42, no. 4, 040401, 2024.

[18]S. J. Shin, et al., "Magnetron sputter deposition of boron carbide in Ne and Ar plasmas," *Journal of Applied Physics*, vol. 135, no. 8, 085303, 2024.

[19]V. Kouznetsov, K. Macak, J. M. Schneider, U. Helmersson, and I. Petrov, "A novel pulsed magnetron sputter technique utilizing very high target power densities," Surf. Coat. Technol. **122**, 290 (1999).

[20]J. T. Gudmundsson, N. Brenning, D. Lundin, and U. Helmersson, "High power impulse magnetron sputtering discharge," J. Vac. Sci. Technol. A **30**, 030801 (2012).

[21]S. Schmidt, et al., "Low-temperature growth of boron carbide coatings by direct current magnetron sputtering and high-power impulse magnetron sputtering," *Journal of Materials Science*, vol. 51, no. 23, pp. 10418, 2016.

[22]A. Aijaz, K. Sarakinos, D. Lundin, N. Brenning, and U. Helmersson, "A strategy for increased carbon ionization in magnetron sputtering discharges," Diamond and Related Materials **23**, 1 (2012).

[23]F. Haase, D. Lundin, S. Bornholdt, and H. Kersten, "On the Impact of Electron Temperature in Magnetron Sputtering Benchmarked with Energy Flux Measurements," Contrib. Plasma Phys. **55**, 701 (2015).

[24]W. C. Oliver and G. M. Pharr. "An improved technique for determining hardness and elastic modulus using load and displacement sensing indentation experiments." J. Mater. Res. 7, 1564 (1992).

[25]S. O. Kucheyev, A. V. Hamza, J. H. Satcher Jr, and M. A. Worsley. "Depth-sensing indentation of low-density brittle nanoporous solids." Acta Mater. 57, 3472 (2009).

[26]S. M. Rossnagel and H. R. Kaufman, "Current–voltage relations in magnetrons," *Journal of Vacuum Science & Technology A*, vol. 6, no. 2, pp. 223, 1988.

[27]I. Petrov, et al., "Comparison of Some Basic Plasma Parameters and Discharge Characteristics of Planar Magnetron Sputtering Discharges in Argon and Neon," *Contributions to Plasma Physics*, vol. 30, no. 2, pp. 223, 1990.

[28]S. J. Shin, J. H. Bae, A. M. Engwall, L. B. Bayu Aji, A. A. Baker, G. V. Taylor, J. B. Merlo, L. R. Sohngen, J. D. Moody, S. O. Kucheyev, Deoposition of ultrathick heavy-metal alloys on rotating substrates by high-power impulse magnetron sputtering: Target erosion effects, J. Appl. Phys. **135**, 035301 (2024).

TABLE I. Conditions and resulting film thicknesses of the two deposition runs of the present study. The substrate tilt angle ($\alpha$) is defined in the text.

| Parameter | Run 1 | Run 2 |
|---|---|---|
| Ne content in Ar-Ne mix (%) | 0 | 10 |
| Peak voltage (V) | 680 | 680 |
| Average power (W) | 210 | 370 |
| Peak target current (A) | 25 | 46 |
| Pulse frequency (Hz) | 50 | 50 |
| Pulse width ($\mu$s) | 500 | 500 |
| Substrate bias (V) | $-25$ | $-25$ |
| Pressure (mTorr) | 45 | 45 |
| Deposition time (h) | 3 | 3 |
| Target-to-substrate distance (mm) | 50 | 50 |
| Film thickness for $\alpha = 0^\circ$ ($\mu$m) | 2.8 | 4.6 |

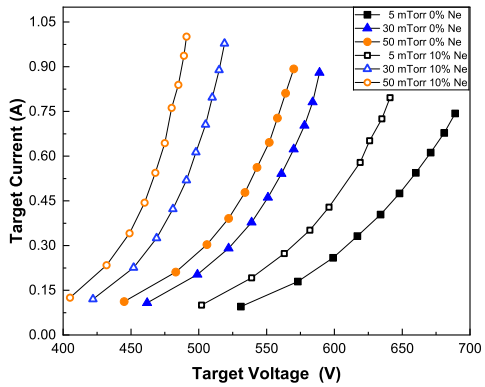


FIG. 1. Dependence of target current on the absolute value of (negative) target voltage for the DCMS discharge in Ar-Ne mixtures with 0 and 10% of Ne at 5, 30, and 50 mTorr, as indicated in the legend.

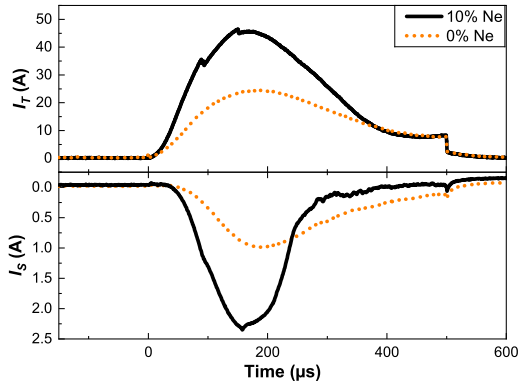


FIG. 2. Waveforms of (a) target current ($I_t$) and (b) substrate current ($I_s$) for Ar-Ne mixtures with 0 and 10% of Ne at 45 mTorr, a peak target voltage of 680 V, and a substrate bias of −25 V. Current of ions from the plasma is shown as positive in both panels. The legend in (a) applies to both panels.

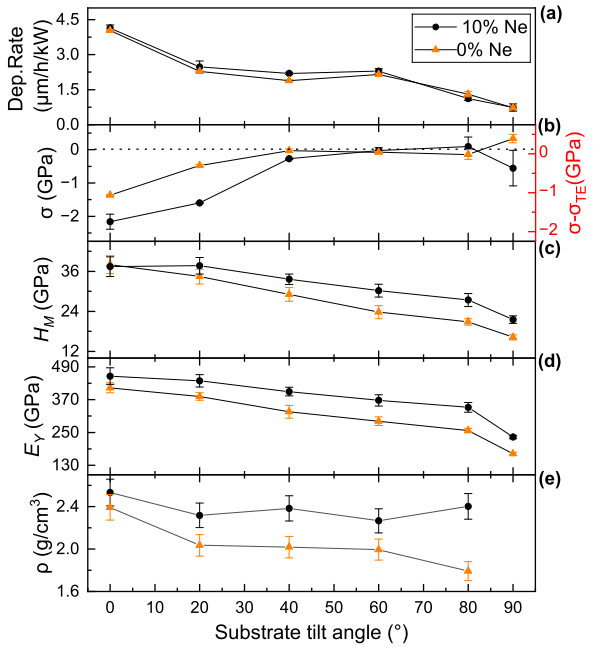


FIG. 3. Substrate tilt dependencies of (a) the deposition rate normalized to the average discharge power, (b) residual stress ($\sigma$, where $\sigma_{TE}$ is the stress contribution due to the thermal expansion mismatch between the substrate and the film), (c) Meyer's Hardness ($H_M$), (d) Young's Modulus ($E_Y$), and (e) mass density ($\rho$) of $B_4C$ films deposited at 45 mTorr in Ar-Ne mixtures with 0 and 10% of Ne, as indicated in the legend in (b), which applies to all five panels.

**Revision #1 of FST24-266**

# High-power impulse magnetron sputter deposition of boron carbide with full-face erosion magnetron and mixed Ar-Ne plasma

G. V. Taylor, S. Graiser, L. B. Bayu Aji, S. J. Shin, D. C. Goodelman, X. Lepro Chavez, and S. O. Kucheyev

*Lawrence Livermore National Laboratory, Livermore, California 94550, U.S.A.*

(Dated: 2 August 2025)

Boron carbide ($B_4C$) is an attractive inertial confinement fusion ablator material. The fabrication of $B_4C$ ablators by magnetron sputtering requires process optimization. To increase process flexibility, here, we explore high-power impulse magnetron sputter (HiPIMS) deposition of $B_4C$ in pure Ar and mixed Ar-Ne plasmas. Results show that higher plasma discharge currents can be reached with a mixed Ar-Ne plasma in the entire working pressure range studied ($5-50$ mTorr). At 45 mTorr with 10% of Ne in the Ar-Ne mix, high peak target current densities of $\sim 1$ A cm$^{-2}$ are demonstrated. Films deposited with such a mixed Ar-Ne plasma with a full face erosion magnetron source on substrates biased at $-25$ V exhibit higher density and improved mechanical properties albeit with higher compressive residual stresses compared to the case of HiPIMS deposition in a pure Ar plasma. This work demonstrates additional process flexibility of the HiPIMS discharge mode for the deposition of $B_4C$ coatings.

## I. INTRODUCTION

The widespread use of boron carbide ($B_4C$) for nuclear, defense, aerospace, and tribological applications is owed to its distinct set of properties.[?] Low density in combination with high mechanical strength, hardness, and chemical stability make $B_4C$ an excellent material for ballistic armor plating[?] and various wear-resistant coatings.[?] In addition, the high neutron absorption cross-section and excellent thermal and mechanical properties make $B_4C$ attractive for nuclear reactor applications, including reaction control rods, neutron detectors, and radiation shielding.[? ?] Moreover, $B_4C$ is an attractive next-generation ablator material for inertial confinement fusion (ICF) and inertial fusion energy (IFE) applications.[? ?] For ICF and IFE, $B_4C$ is required in the form of hollow spherical shells with a diameter of $\sim 0.5 - 5.0$ mm and a wall thickness of $\sim 20 - 200$ $\mu$m.[?]

Magnetron sputtering[?] is currently the leading method for the fabrication of such spherical $B_4C$ shells for ICF and IFE.[? ? ?] It is a highly repeatable and scalable physical vapor deposition technique with a large and tunable parameter space.[?] It is used in many industries to deposit both metals and ceramics. Recent developments in magnetron sputtering of $B_4C$ include systematic studies of working gas pressure,[? ?] substrate temperature,[? ?] substrate tilt angles,[? ? ? ? ?] and plasma composition[? ?] on film properties. A significant reduction in the density of nodular defects has been demonstrated for $B_4C$ films deposited with a full face erosion (FFE) magnetron source.[?] A follow up work[?] has explored the FFE source deposition of $B_4C$ onto rolling spherical substrates, as required for ICF ablator capsule fabrication. All these previous studies[? ? ? ? ? ? ? ? ?] have used either the direct current magnetron sputtering (DCMS) or radio-frequency magnetron sputtering (RFMS) plasma discharge mode.

High-power impulse magnetron sputtering (HiPIMS)[? ?] is another plasma discharge mode offering expanded process flexibility compared to conventional DCMS and RFMS modes. Schmidt *et al.*[?] have evaluated HiPIMS deposition of $B_4C$, with the focus on effects of Ar working gas pressure at two substrate temperatures of 100 and 400 °C. They have compared films deposited by DCMS and HiPIMS discharge modes, with relatively low peak target current densities of $\sim 0.16$ A cm$^{-2}$. They found a negligible difference in properties of films deposited onto electrically floating substrates by DCMS or HiPIMS. Their results suggest that, for such low peak target current densities and their specific experimental con-

ditions, HiPIMS adds process complexity but offers no advantage over conventional DCMS.

Here, we explore the capabilities of HiPIMS deposition of $B_4C$ by capitalizing on our recent findings of reduced nodular defect densities in films deposited with FFE magnetrons[?] and higher discharge current densities for Ne-containing plasmas.[?] The addition of Ne to a predominantly Ar plasma has also been demonstrated to increase electron temperature and, hence, the degree of ionization of of depositing species flux.[? ?] We use an FFE magnetron source operated in the HiPIMS mode and compare properties of films deposited on negatively biased substrates with different tilt angles in pure Ar and mixed Ar-Ne plasmas with peak target current densities of $\sim 1$ A cm$^{-2}$. The understanding of oblique angle deposition effects is directly relevant to ICF and IFE ablator fabrication since it involves the deposition onto non-planar (spherical) substrates.[?] Our results demonstrate that HiPIMS offers additional process flexibility for $B_4C$ deposition and warrants further systematic studies.

## II. METHODS

Table **??** summarizes deposition conditions for the two coating runs of the present study. Coatings were deposited in a cylindrical high-vacuum chamber with a diameter and height of 44 and 36 cm, respectively. Prior to admitting working gases into the chamber, the substrate holder was heated to 450 °C, corresponding to a substrate temperature of 330 °C, and the chamber pressure was $\sim 5 \times 10^{-6}$ Torr. Our previous study[?] has found negligible effects of the residual chamber pressure, in the range of $(5 - 200) \times 10^{-7}$ Torr, on the elemental composition of sputter deposited $B_4C$ films. Depositions were performed with a 75-mm diameter circular FFE magnetron source (Gencoa Ltd, model FFE-75, UK) modified for direct target cooling. The source axis was positioned horizontally. Disk-shaped $B_4C$ targets (Feldco International, USA) had a diameter of 71 mm, an initial thickness of 3 mm, a density of 2.4 g cm$^3$ and an electrical resistivity of $\sim 2 \times 10^4$ Ω cm. Disks of $B_4C$ were bonded with In to 2-mm-thick Mo backing plates. The total thickness of the bonded target assembly at the thinnest point of the racetrack before and after each deposition experiment was in the range of $4.84 - 4.91$ mm. The DC plasma was driven with an Advanced Energy MDX 1K power supply unit. The HiPIMS plasma was driven with an Advanced Energy MDX 1K power supply unit, which was coupled to a high-voltage pulser unit (Ionautics, model HiSPTER 1, Sweden). The two deposition runs described here were done in the constant

peak target voltage mode.

Depositions were performed with high purity Ar (99.998 %) and Ne (99.998 %) gases. Following a survey of various partial pressures of Ne, we used an Ar-Ne mix with 10% of Ne and a long pulse duration as it resulted in a stable plasma discharge at 45 mTorr. Such a relatively high working gas pressure of 45 mTorr was also chosen to minimize compressive residual stress in films, based on our previous study.[?] The total working gas flow rate was 55 standard cubic centimeters per minute. Prior to each run, a 30-minute pre-conditioning of the target was performed at the set point parameters with the substrates shielded from the target by an electrically grounded shutter.

Substrates were mounted on a custom-designed faceted substrate holder machined from a solid Mo block, which was described previously.[?] Heating of the substrate holder was achieved with an electrically grounded resistive heater (HeatWave Labs Inc., model 112868, USA). Substrates were mechanically clamped to the holder with Mo screws and washers. In this configuration, the normal of substrate holder facets were at the following angles ($\alpha$) to the magnetron source axis: 0°, 20°, 40°, 60°, 80°, and 90°. The two substrate types used were (i) $10 \times 10$ mm$^2$ Si (100) chips with a 200-nm-thick Ta metal layer deposited on top in a separate DCMS run used for density measurements and (ii) $3 \times 12$ mm$^2$, 280 $\mu$m thick Si (100) cantilevers used for residual stress, mechanical properties, and deposition rate measurements. Due to design restrictions of the faceted substrate holder, chips were only included on facets with $\alpha = 0 - 80°$, while cantilevers were placed on all six facets. To ensure consistent initial substrate cleanliness, we used the following three-step substrate cleaning procedure in an ultrasonic bath (with 15 minutes for each step): (i) acetone, (ii) ethanol, and (iii) a water-based detergent solution. This was followed by a final rinse in de-ionized water and blow drying with dry nitrogen.

Film thickness was measured by stylus profilometry (Bruker, model Dektak XT, USA). Residual stress in films was calculated with the Stoney equation based on the change in cantilever curvature measured by profilometry before and after deposition. The thermal stress component originating from the difference in coefficients of thermal expansion between the $B_4C$ film and Si substrate was estimated to be 100 MPa (tensile), as in our previous studies.[? ?] The Ta layer on Si chips was used as a marker in the areal density measurements by Rutherford backscattering spectrometry (RBS) with a 2 MeV $^1H^+$ ion beam. The presence of this Ta marker layer has a negligible effect on the properties and

morphology of $B_4C$ films deposited as substrate temperatures of the present study.[?]

Mechanical properties were evaluated by nanoindentation (MTS, model XP, USA) in the load-controlled mode with a Berkovich diamond tip. Meyer's hardness ($H_M$) was defined as average contact pressure, and Young's Modulus ($E_Y$) was calculated based on the conventional Oliver-Pharr method.[?] In Oliver-Pharr calculations, we assumed Poisson's ratios of diamond and $B_4C$ films of 0.07 and 0.17, respectively, and Young's modulus of diamond of 1141 GPa.[?] Values of $H_M$ and $E_Y$ were averaged over the indenter penetration depth range of $\sim 10 - 20\%$ of film thickness.

## III. RESULTS AND DISCUSSION

### A. Discharge characteristics

Figure **??** shows dependencies of DCMS plasma discharge target current ($I_t$) versus target voltage ($V_t$) for Ar-Ne mixes with 0 and 10% of Ne, collected at three representative working pressures. In the entire pressure range studied of $5 - 50$ mTorr, for both gas mixes, the discharge behavior is qualitatively similar. All $I_t(V_t)$ curves are superlinear, as commonly observed for Ar magnetron discharges[?] and different from the abnormal $I_t(V_t)$ dependence characteristic of the discharge with a pure Ne plasma.[?]

As working pressure is increased, Fig. **??** shows that $I_t$ at any given $V_t$ increases. Hence, higher $I_t$ values at lower voltages can be achieved at larger working pressures. While this general trend is the same for Ar-Ne mixes with 0 and 10% of Ne, the effect of pressure on the $I_t(V_t)$ dependence is significantly larger for the 10% Ne case. This could be attributed to a combination of (i) a reduction in rarefaction[?] near the target surface due to the higher thermal conductivity and smaller collisional cross section of Ne compared to Ar and (ii) a higher secondary ion-electron emission coefficient of Ne.[? ?] It is seen from Fig. **??** that, for a given $V_t$, larger $I_t$ is achieved for higher pressure with 10% of Ne in the mix. Hence, we chose these conditions for HiPIMS film deposition runs of the present study (Table **??**).

Figure **??** shows waveforms of $I_t$ [Fig. **??**(a)] and substrate current [$I_s$, Fig. **??**(b)] for Ar-Ne mixtures with 0 and 10% of Ne with at 45 mTorr. For both working gas configurations, the HiPIMS waveforms have peak target currents that are two-orders of magnitude greater than their DCMS counterparts at similar average discharge power (Fig. **??**). It is also seen

from Fig. **??**(a) that the admix of Ne to the plasma helps achieve higher peak currents. The peak $I_t$ and $I_s$ for the 10% of Ne mix are $\sim 2$ times those for the 0% Ne case, leading to a higher plasma density and larger flux of ions bombarding the film surface during growth with the Ne-containing plasma.

The shape of $V_t$ and $V_s$ waveforms in Figs. **??**(a) and **??**(b) are qualitatively the same. They exhibit a gradual increase to a peak at $\sim 150$ $\mu$s from the pulse start, followed by a decrease and saturation for $\gtrsim 400$ $\mu$s. This waveform shape is qualitatively similar to those revealed in our recent systematic study of HiPIMS deposition of Au-Ta alloys with 2-inch MAK-model magnetron sources.[?] However, the time scales are $\sim 4$ times slower for the $B_4C$ discharge. This is an interesting observation with practical implications for deposition process optimization, and more work is clearly needed to better understand $B_4C$ HiPIMS plasma and deposition processes.

## B. Film properties

Figure **??**(a) shows the substrate tilt angle ($\alpha$) dependence of the deposition rate. The rate has been normalized by the average discharge power in order to compare results for two runs with 0 and 10% of Ne in the Ar-Ne mix performed at constant peak target voltage and different peak $I_t$ and average discharge power values (Table **??**). It is seen from Fig. **??**(a) that, for both cases of 0 and 10% of Ne, the deposition rates are essentially identical. Interestingly, the rapid decrease in the deposition rate with increasing $\alpha$ observed in several previous investigations[? ? ? ?] of DCMS and RFMS deposition of $B_4C$ is not seen in Fig. **??**(a). Instead, a decrease in the deposition rate occurs between $\alpha = 0°$ and 20°, followed by a nearly constant rate for $\alpha$ in the range of $20 - 60°$, and then another decrease for strongly oblique angles of $\alpha = 80$ and 90°. This observation may result from a combination of high working pressure of 45 mTorr, resulting in efficient scattering of depositing species flux, and ion extraction through the substrate plasma sheath due to the electric field generated from the negative substrate bias. A follow up systematic investigation of depositing species flux as well their energy and angular distributions could help better understand this unexpected behavior.

Figure **??**(b) shows the $\alpha$ dependence of residual stress ($\sigma$), revealing that, compared to the case of pure Ar plasma deposition, films deposited with a 10% Ne mix have higher

compressive $\sigma$ for low $\alpha$ cases of 0 and 20°. For example, for untilted films, compressive $\sigma$ increases from 1.4 to 2.2 GPa with the addition of Ne to the plasma. This can be attributed to a corresponding increase in ion flux [Fig. **??**(b)]. For both plasma conditions, $\sigma$ is close to zero for $\alpha$ of 40° and above. This suggests that the growth of films at such oblique angles is dominated by oblique angle atomic impacts resulting in a columnar microstructure with low residual stress.[?]

As shown in Fig. **??**(c), high hardness values ($H_M$ = 38 GPa) are measured in coatings from both runs for the $\alpha = 0°$ tilt angle. For larger $\alpha$ films, $H_M$ values for 0 and 10% of Ne cases diverge. Films deposited with 10% of Ne have consistently higher $H_M$ values. The same trend is replicated by the $\alpha$ dependence of $E_Y$ shown in Fig. **??**(d). Films deposited with a 10% of Ne are stiffer. This trend could be explained by examining the evolution of film density shown in Fig. **??**(e). It reveals that films deposited with the Ne-containing plasma have higher density although their their normalized deposition rates are largely the same [Fig. **??**(a)]. This suggests that the deposition with a Ne-containing plasma is characterized by an increased target sputtering rate. Films deposited with a 100% Ar plasma have a density of 2.4 g/cm$^3$ at $\alpha = 0°$, $\sim$ 2.0 g/cm$^3$ for $\alpha$ in the range of $0 - 60°$, and 1.8 g/cm$^{-3}$ for $\alpha = 80°$. Films deposited with a 10% Ne mix exhibit a similar trend but with overall higher density values. Overall, the density in films is shown to be weakly dependent on substrate tilt angle, and this is especially the case for the 10% Ne samples. This behavior could be attributed to a larger ion-to-atom fraction and more efficient ion bombardment of the growing film surface for the case of Ne-containing plasma although additional systematic studies involving plasma diagnostics are currently needed to better understand film growth mechanisms and optimize the deposition process.

## IV. SUMMARY

We have used magnetron sputtering to deposit $B_4C$ films with an FFE source modified for direct cooling with the HiPIMS plasma discharge mode with two different working gases (pure Ar and an Ar-Ne mix with 10% of Ne) and substrates biased at $-25$ V. Higher plasma densities, as indicated by larger target and substrate currents, can be achieved by using larger process pressure and adding Ne to the working gas mixture. This work has demonstrated that the density and mechanical properties of $B_4C$ films can be improved with

the deposition in the HiPIMS mode in an Ar-Ne working gas mix. Our results demonstrate that the HiPIMS discharge mode coupled with Ar-Ne gas mixture expands the flexibility of magnetron sputter deposition of $B_4C$ and offers additional process control. However, it also increases process complexity, and more work is currently needed to better understand the physics of the HiPIMS $B_4C$ mixed plasma discharge with an FFE magnetron source.

## V. ACKNOWLEDGMENTS

This work was performed under the auspices of the U.S. DOE by LLNL under Contract DE-AC52-07NA27344.

## VI. DATA AVAILABILITY STATEMENT

The data that supports the findings of this study is available within the article.

## VII. AUTHOR DECLARATIONS

### A. Conflict of Interest

The authors have no conflicts to disclose.

## REFERENCES


[1]F. Thévenot, "Boron carbide—A comprehensive review," *Journal of the European Ceramic Society*, vol. 6, no. 4, pp. 205, 1990.

[2]S. G. Savio, et al., "An experimental study on ballistic performance of boron carbide tiles," *International Journal of Impact Engineering*, vol. 38, no. 7, pp. 535, 2011.

[3]S. Bhatia, et al., "A review on mechanical and tribological characterization of boron carbide reinforced epoxy composite," *Advanced Composite Materials*, vol. 30, no. 4, pp. 307, Taylor & Francis, 2021.

[4]B. S. Gajjar, et al., "Boron Carbide as High-Energy Radiation Shielding Material for ITER," *IEEE Transactions on Plasma Science*, vol. 50, no. 12, pp. 5078, 2022.

[5]Y. Q. Chen and B. H. Yan, "The technology of shielding design for nuclear reactor: A review," *Progress in Nuclear Energy*, vol. 161, 104741, 2023.

[6]S. W. Haan, et al., "Design and modeling of ignition targets for the National Ignition Facility," Physics of Plasmas, vol. 2, no. 6, pp. 2480, 1995.

[7]T. R. Dittrich, S. W. Haan, S. Pollaine, A. K. Burnham, and G. L. Strobel, "NIF capsule design update," Fusion Sci. Tech. **31**, 402 (1997).

[8]S. O. Kucheyev, et al., "Development of New Magnetron Sputter Deposition Processes for Laser Target Fabrication," *Fusion Science and Technology*, vol. 79, no. 7, pp. 823, American Nuclear Society, 2023.

[9]W. D. Westwood, Sputter deposition, AVS, New York (2003).

[10]A. K. Burnham, C. S. Alford, D. M. Makowiecki, T. R. Dittrich, R. J. Wallace, E. C. Honea, and C. M. King, "Evaluation of B4C as an Ablator Material for NIF Capsules," Fusion Sci. Tech. **31**, 456 (1997).

[11]J. B. Merlo, et al., "Magnetron sputter deposition of ultrathick boron carbide coatings on spherical substrates for inertial confinement fusion," *Surface and Coatings Technology*, vol. 477, 130321, 2024.130321.

[12]A. M. Engwall, L. B. Bayu Aji, S. Shin, P. B. Mirkarimi, J. H. Bae, and S. O. Kucheyev, J. Appl. Phys. **128**, 175301 (2020).

[13]L. B. Bayu Aji, et al., "Radio-frequency magnetron sputter deposition of ultrathick boron carbide films," *Journal of Vacuum Science & Technology A*, vol. 41, no. 2, 023407, 2023.

[14]L. B. Bayu Aji, et al., "Effect of substrate temperature on sputter-deposited boron carbide films," *Journal of Applied Physics*, vol. 131, no. 7, 075304, 2022.

[15]S. J. Shin, L. B. Bayu Aji, A. M. Engwall, J. H. Bae, G. V. Taylor, P. B. Mirkarimi, C. Aracne-Ruddle, J. Nguyen, C. W. N. Kong, and S. O. Kucheyev, Fusion Sci. Technol. **79**, 841 (2023).

[16]S. J. Shin, et al., "Oblique angle deposition of boron carbide films by magnetron sputtering," *Journal of Applied Physics*, vol. 130, no. 12, 125305, 2021.

[17]G. V. Taylor, et al., "Boron carbide films with reduced nodular defect density deposited by full-face erosion radio-frequency magnetron sputtering," *Journal of Vacuum Science & Technology A*, vol. 42, no. 4, 040401, 2024.

[18]S. J. Shin, et al., "Magnetron sputter deposition of boron carbide in Ne and Ar plasmas," *Journal of Applied Physics*, vol. 135, no. 8, 085303, 2024.

[19]V. Kouznetsov, K. Macak, J. M. Schneider, U. Helmersson, and I. Petrov, "A novel pulsed magnetron sputter technique utilizing very high target power densities," Surf. Coat. Technol. **122**, 290 (1999).

[20]J. T. Gudmundsson, N. Brenning, D. Lundin, and U. Helmersson, "High power impulse magnetron sputtering discharge," J. Vac. Sci. Technol. A **30**, 030801 (2012).

[21]S. Schmidt, et al., "Low-temperature growth of boron carbide coatings by direct current magnetron sputtering and high-power impulse magnetron sputtering," *Journal of Materials Science*, vol. 51, no. 23, pp. 10418, 2016.

[22]A. Aijaz, K. Sarakinos, D. Lundin, N. Brenning, and U. Helmersson, "A strategy for increased carbon ionization in magnetron sputtering discharges," Diamond and Related Materials **23**, 1 (2012).

[23]F. Haase, D. Lundin, S. Bornholdt, and H. Kersten, "On the Impact of Electron Temperature in Magnetron Sputtering Benchmarked with Energy Flux Measurements," Contrib. Plasma Phys. **55**, 701 (2015).

[24]W. C. Oliver and G. M. Pharr. "An improved technique for determining hardness and elastic modulus using load and displacement sensing indentation experiments." J. Mater. Res. 7, 1564 (1992).

[25]S. O. Kucheyev, A. V. Hamza, J. H. Satcher Jr, and M. A. Worsley. "Depth-sensing indentation of low-density brittle nanoporous solids." Acta Mater. 57, 3472 (2009).

[26]S. M. Rossnagel and H. R. Kaufman, "Current–voltage relations in magnetrons," *Journal of Vacuum Science & Technology A*, vol. 6, no. 2, pp. 223, 1988.

[27]I. Petrov, et al., "Comparison of Some Basic Plasma Parameters and Discharge Characteristics of Planar Magnetron Sputtering Discharges in Argon and Neon," *Contributions to Plasma Physics*, vol. 30, no. 2, pp. 223, 1990.

[28]S. J. Shin, J. H. Bae, A. M. Engwall, L. B. Bayu Aji, A. A. Baker, G. V. Taylor, J. B. Merlo, L. R. Sohngen, J. D. Moody, S. O. Kucheyev, Deoposition of ultrathick heavy-metal alloys on rotating substrates by high-power impulse magnetron sputtering: Target erosion effects, J. Appl. Phys. **135**, 035301 (2024).

TABLE I. Conditions and resulting film thicknesses of the two deposition runs of the present study. The substrate tilt angle ($\alpha$) is defined in the text.

| Parameter | Run 1 | Run 2 |
|---|---|---|
| Ne content in Ar-Ne mix (%) | 0 | 10 |
| Peak voltage (V) | 680 | 680 |
| Average power (W) | 210 | 370 |
| Peak target current (A) | 25 | 46 |
| Pulse frequency (Hz) | 50 | 50 |
| Pulse width ($\mu$s) | 500 | 500 |
| Substrate bias (V) | $-25$ | $-25$ |
| Pressure (mTorr) | 45 | 45 |
| Deposition time (h) | 3 | 3 |
| Target-to-substrate distance (mm) | 50 | 50 |
| Film thickness for $\alpha = 0^\circ$ ($\mu$m) | 2.8 | 4.6 |

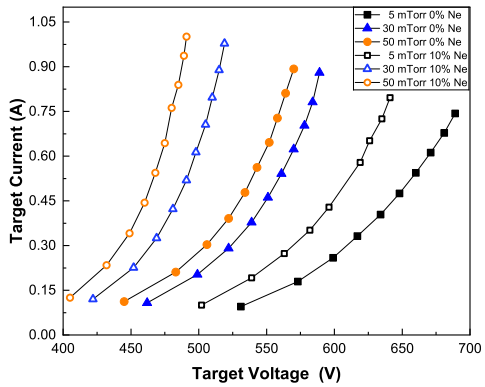


FIG. 1. Dependence of target current on the absolute value of (negative) target voltage for the DCMS discharge in Ar-Ne mixtures with 0 and 10% of Ne at 5, 30, and 50 mTorr, as indicated in the legend.

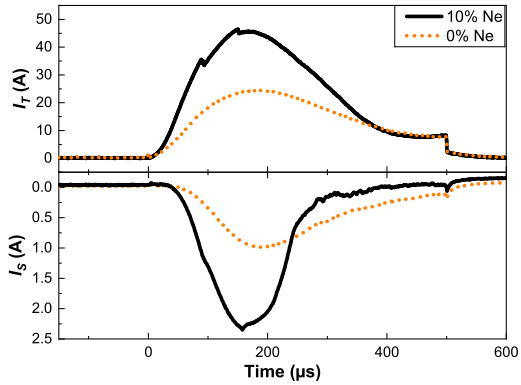


FIG. 2. Waveforms of (a) target current ($I_t$) and (b) substrate current ($I_s$) for Ar-Ne mixtures with 0 and 10% of Ne at 45 mTorr, a peak target voltage of 680 V, and a substrate bias of −25 V. Current of ions from the plasma is shown as positive in both panels. The legend in (a) applies to both panels.

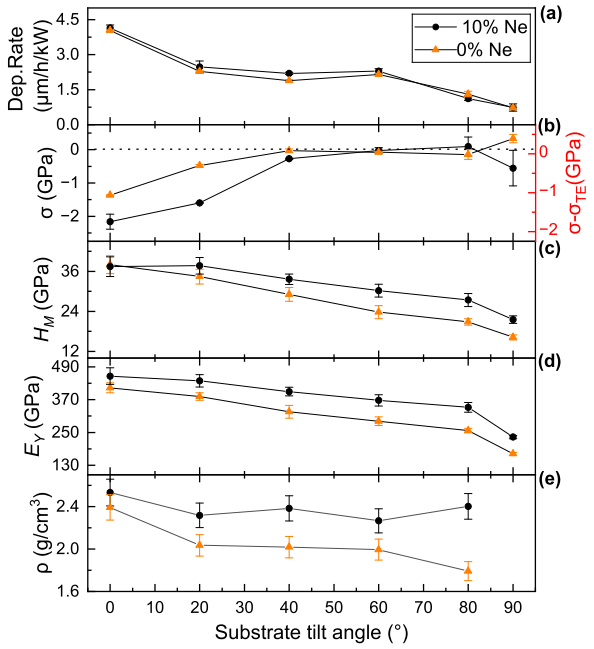


FIG. 3. Substrate tilt dependencies of (a) the deposition rate normalized to the average discharge power, (b) residual stress ($\sigma$, where $\sigma_{TE}$ is the stress contribution due to the thermal expansion mismatch between the substrate and the film), (c) Meyer's Hardness ($H_M$), (d) Young's Modulus ($E_Y$), and (e) mass density ($\rho$) of $B_4C$ films deposited at 45 mTorr in Ar-Ne mixtures with 0 and 10% of Ne, as indicated in the legend in (b), which applies to all five panels.

**Revision #1 of FST24-266 with corrections indicated**

# High-power impulse magnetron sputter deposition of boron carbide with full-face erosion magnetron and mixed Ar-Ne plasma

G. V. Taylor, S. Graiser, L. B. Bayu Aji, S. J. Shin, D. C. Goodelman, X. Lepro Chavez, and S. O. Kucheyev

*Lawrence Livermore National Laboratory, Livermore, California 94550, U.S.A.*

(Dated: 1 August 2025)

Boron carbide ($B_4C$) is an attractive inertial confinement fusion ablator material. The fabrication of $B_4C$ ablators by magnetron sputtering requires process optimization. To increase process flexibility, here, we explore high-power impulse magnetron sputter (HiPIMS) deposition of $B_4C$ in pure Ar and mixed Ar-Ne plasmas. Results show that higher plasma discharge currents can be reached with a mixed Ar-Ne plasma in the entire working pressure range studied ($5-50$ mTorr). At 45 mTorr with 10% of Ne in the Ar-Ne mix, high peak target current densities of $\sim 1$ A cm$^{-2}$ are demonstrated. Films deposited with such a mixed Ar-Ne plasma with a full face erosion magnetron source on substrates biased at $-25$ V exhibit higher density and improved mechanical properties albeit with higher compressive residual stresses compared to the case of HiPIMS deposition in a pure Ar plasma. This work demonstrates additional process flexibility of the HiPIMS discharge mode for the deposition of $B_4C$ coatings.

## I. INTRODUCTION

The widespread use of boron carbide ($B_4C$) for nuclear, defense, aerospace, and tribological applications is owed to its distinct set of properties.[1] Low density in combination with high mechanical strength, hardness, and chemical stability make $B_4C$ an excellent material for ballistic armor plating[2] and various wear-resistant coatings.[3] In addition, the high neutron absorption cross-section and excellent thermal and mechanical properties make $B_4C$ attractive for nuclear reactor applications, including reaction control rods, neutron detectors, and radiation shielding.[4,5] Moreover, $B_4C$ is an attractive next-generation ablator material for inertial confinement fusion (ICF) and inertial fusion energy (IFE) applications.[6,7] For ICF and IFE, $B_4C$ is required in the form of hollow spherical shells with a diameter of $\sim 0.5 - 5.0$ mm and a wall thickness of $\sim 20 - 200$ $\mu$m.[8]

Magnetron sputtering[9] is currently the leading method for the fabrication of such spherical $B_4C$ shells for ICF and IFE.[8,10,11] It is a highly repeatable and scalable physical vapor deposition technique with a large and tunable parameter space.[9] It is used in many industries to deposit both metals and ceramics. Recent developments in magnetron sputtering of $B_4C$ include systematic studies of working gas pressure,[12,13] substrate temperature,[8,14] substrate tilt angles,[8,13,15–17] and plasma composition[15,18] on film properties. A significant reduction in the density of nodular defects has been demonstrated for $B_4C$ films deposited with a full face erosion (FFE) magnetron source.[17] A follow up work[11] has explored the FFE source deposition of $B_4C$ onto rolling spherical substrates, as required for ICF ablator capsule fabrication. All these previous studies[8,11–18] have used either the direct current magnetron sputtering (DCMS) or radio-frequency magnetron sputtering (RFMS) plasma discharge mode.

High-power impulse magnetron sputtering (HiPIMS)[19,20] is another plasma discharge mode offering expanded process flexibility compared to conventional DCMS and RFMS modes. Schmidt *et al.*,[21] have evaluated HiPIMS deposition of $B_4C$, with the focus on effects of Ar working gas pressure at two substrate temperatures of 100 and 400 °C. They have compared films deposited by DCMS and HiPIMS discharge modes, with relatively low peak target current densities of $\sim 0.16$ A cm$^{-2}$. They found a negligible difference in properties of films deposited onto electrically floating substrates by DCMS or HiPIMS. Their results suggest that, for such low peak target current densities and their specific experimental

conditions, HiPIMS ~~add~~ adds process complexity but offers no advantage over conventional DCMS.

Here, we explore the capabilities of HiPIMS deposition of $B_4C$ by capitalizing on our recent findings of reduced nodular defect densities in films deposited with FFE magnetrons[17] and higher discharge current densities for Ne-containing plasmas.[18] The addition of Ne to a predominantly Ar plasma has also been demonstrated to increase electron temperature and, hence, the degree of ionization of of depositing species flux. [22,23] We use an FFE magnetron source operated in the HiPIMS mode and compare properties of films deposited on negatively biased substrates with different tilt angles in pure Ar and mixed Ar-Ne plasmas with peak target current densities of $\sim 1$ A cm$^{-2}$. The understanding of oblique angle deposition effects is directly relevant to ICF and IFE ablator fabrication since it involves the deposition onto non-planar (spherical) substrates. [8] Our results demonstrate that HiPIMS offers additional process flexibility for $B_4C$ deposition and warrants further systematic studies.

## II. METHODS

Table I summarizes deposition conditions for the two coating runs of the present study. Coatings were deposited in a cylindrical high-vacuum chamber with a diameter and height of 44 and 36 cm, respectively. Prior to admitting working gases into the chamber, the substrate holder was heated to 450 °C, corresponding to a substrate temperature of 330 °C, and the chamber pressure was $\sim 5 \times 10^{-6}$ Torr. Our previous study [14] has found negligible effects of the residual chamber pressure, in the range of $(5 - 200) \times 10^{-7}$ Torr, on the elemental composition of sputter deposited $B_4C$ films. Depositions were performed with a 75-mm diameter circular FFE magnetron source (Gencoa Ltd, model FFE-75, UK) modified for direct target cooling. The source axis was positioned horizontally. Disk-shaped $B_4C$ targets (Feldco International, USA) had a diameter of 71 mm, an initial thickness of 3 mm, a density of 2.4 g cm$^3$ and an electrical resistivity of $\sim 2 \times 10^4$ Ω cm. Disks of $B_4C$ were bonded with In to 2-mm-thick Mo backing plates. The total thickness of the bonded target assembly at the thinnest point of the racetrack before and after each deposition experiment was in the range of $4.84 - 4.91$ mm. The DC plasma was driven with an Advanced Energy MDX 1K power supply unit. The HiPIMS plasma was driven with an Advanced Energy MDX 1K power supply unit, which was coupled to a high-voltage pulser unit (Ionautics, model

HiSPTER 1, Sweden). The two deposition runs described here were done in the constant peak target voltage mode.

Depositions were performed with high purity Ar (99.998 %) and Ne (99.998 %) gases. Following a survey of various partial pressures of Ne, we used an Ar-Ne mix with 10% of Ne and a long pulse duration as it resulted in a stable plasma discharge ~~.~~ at 45 mTorr. Such a relatively high working gas pressure of 45 mTorr was also chosen to minimize compressive residual stress in films, based on our previous study. [12] The total working gas flow rate was 55 standard cubic centimeters per minute. Prior to each run, a 30-minute pre-conditioning of the target was performed at the set point parameters with the substrates shielded from the target by an electrically grounded shutter.

Substrates were mounted on a custom-designed faceted substrate holder machined from a solid Mo block, which was described previously.[16] Heating of the substrate holder was achieved with an electrically grounded resistive heater (HeatWave Labs Inc., model 112868, USA). Substrates were mechanically clamped to the holder with Mo screws and washers. In this configuration, the normal of substrate holder facets were at the following angles ($\alpha$) to the magnetron source axis: 0°, 20°, 40°, 60°, 80°, and 90°. The two substrate types used were (i) $10 \times 10$ mm$^2$ Si (100) chips with a 200-nm-thick Ta metal layer deposited on top in a separate DCMS run used for density measurements and (ii) $3 \times 12$ mm$^2$, 280 $\mu$m thick Si (100) cantilevers used for residual stress~~measurements.~~, mechanical properties, and deposition rate measurements. Due to design restrictions of the faceted substrate holder, chips were only included on facets with $\alpha = 0 - 80°$, while cantilevers were placed on all six facets. To ensure consistent initial substrate cleanliness, we used the following three-step substrate cleaning procedure in an ultrasonic bath (with 15 minutes for each step): (i) acetone, (ii) ethanol, and (iii) a water-based detergent solution. This was followed by a final rinse in de-ionized water and blow drying with dry nitrogen.

Film thickness was measured by stylus profilometry (Bruker, model Dektak XT, USA). Residual stress in films was calculated with the Stoney equation based on the change in cantilever curvature measured by profilometry before and after deposition. The thermal stress component originating from the difference in coefficients of thermal expansion between the $B_4C$ film and Si substrate was estimated to be 100 MPa (tensile), as in our previous studies.[16,17] The Ta layer on Si chips was used as a marker in the areal density measurements by Rutherford backscattering spectrometry (RBS) with a 2 MeV $^1H^+$ ion

beam. The presence of this Ta marker layer has a negligible effect on the properties and morphology of $B_4C$ films deposited as substrate temperatures of the present study.[8]

Mechanical properties were evaluated by nanoindentation (MTS, model XP, USA) in the load-controlled mode with a Berkovich diamond tip. Meyer's hardness ($H_M$) was defined as average contact pressure, and Young's Modulus ($E_Y$) was calculated based on the conventional Oliver-Pharr method.[24] In Oliver-Pharr calculations, we assumed Poisson's ratios of diamond and $B_4C$ films of 0.07 and 0.17, respectively, and Young's modulus of diamond of 1141 GPa.[25] Values of $H_M$ and $E_Y$ were averaged over the indenter penetration depth range of $\sim 10 - 20\%$ of film thickness.

## III. RESULTS AND DISCUSSION

### A. Discharge characteristics

Figure 1 shows dependencies of DCMS plasma discharge target current ($I_t$) versus target voltage ($V_t$) for Ar-Ne mixes with 0 and 10% of Ne, collected at three representative working pressures. In the entire pressure range studied of $5 - 50$ mTorr, for both gas mixes, the discharge behavior is qualitatively similar. All $I_t(V_t)$ curves are superlinear, as commonly observed for Ar magnetron discharges[9] and different from the abnormal $I_t(V_t)$ dependence characteristic of the discharge with a pure Ne plasma.[18]

As working pressure is increased, Fig. 1 shows that $I_t$ at any given $V_t$ increases. Hence, higher $I_t$ values at lower voltages can be achieved at larger working pressures. While this general trend is the same for Ar-Ne mixes with 0 and 10% of Ne, the effect of pressure on the $I_t(V_t)$ dependence is significantly larger for the 10% Ne case. This could be attributed to a combination of (i) a reduction in rarefaction[26] near the target surface due to the higher thermal conductivity and smaller collisional cross section of Ne compared to Ar and (ii) a higher secondary ion-electron emission coefficient of Ne.[18,27] It is seen from Fig. 1 that, for a given $V_t$, larger $I_t$ is achieved for higher pressure with 10% of Ne in the mix. Hence, we chose these conditions for HiPIMS film deposition runs of the present study (Table I).

Figure 2 shows waveforms of $I_t$ [Fig. 2(a)] and substrate current [$I_s$, Fig. 2(b)] for Ar-Ne mixtures with 0 and 10% of Ne with at 45 mTorr. For both working gas configurations, the HiPIMS waveforms have peak target currents that are two-orders of magnitude greater than

their DCMS counterparts at similar average discharge power (Fig. 1). It is also seen from Fig. 2(a) that the admix of Ne to the plasma helps achieve higher peak currents. The peak $I_t$ and $I_s$ for the 10% of Ne mix are $\sim 2$ times those for the 0% Ne case, leading to a higher plasma density and larger flux of ions bombarding the film surface during growth with the Ne-containing plasma.

The shape of $V_t$ and $V_s$ waveforms in Figs. 2(a) and 2(b) are qualitatively the same. They exhibit a gradual increase to a peak at $\sim 150$ $\mu$s from the pulse start, followed by a decrease and saturation for $\gtrsim 400$ $\mu$s. This waveform shape is qualitatively similar to those revealed in our recent systematic study of HiPIMS deposition of Au-Ta alloys with 2-inch MAK-model magnetron sources.[28] However, the time scales are $\sim 4$ times slower for the $B_4C$ discharge. This is an interesting observation with practical implications for deposition process optimization, and more work is clearly needed to better understand $B_4C$ HiPIMS plasma and deposition processes.

## B. Film properties

Figure 3(a) shows the substrate tilt angle ($\alpha$) dependence of the deposition rate. The rate has been normalized by the average discharge power in order to compare results for two runs with 0 and 10% of Ne in the Ar-Ne mix performed at constant peak target voltage and different peak $I_t$ and average discharge power values (Table I). It is seen from Fig. 3(a) that, for both cases of 0 and 10% of Ne, the deposition rates are essentially identical. Interestingly, the rapid decrease in the deposition rate with increasing $\alpha$ observed in several previous investigations[13,16–18] of DCMS and RFMS deposition of $B_4C$ is not seen in Fig. 3(a). Instead, a decrease in the deposition rate occurs between $\alpha = 0°$ and 20°, followed by a nearly constant rate for $\alpha$ in the range of $20 - 60°$, and then another decrease for ~~a strongly oblique angle of $\alpha = 80$~~strongly oblique angles of $\alpha = 80$ and 90°. This observation may result from a combination of high working pressure of 45 mTorr, resulting in efficient scattering of depositing species flux, and ion extraction through the substrate plasma sheath due to the electric field generated from the negative substrate bias. A follow up systematic investigation of depositing species flux as well their energy and angular distributions could help better understand this unexpected behavior.

Figure 3(b) shows the $\alpha$ dependence of residual stress ($\sigma$), revealing that, compared to

the case of pure Ar plasma deposition, films deposited with a 10% Ne mix have higher compressive $\sigma$ for low $\alpha$ cases of 0 and 20°. For example, for untilted films, compressive $\sigma$ increases from 1.4 to 2.2 GPa with the addition of Ne to the plasma. This can be attributed to a corresponding increase in ion flux [Fig. 2(b)]. For both plasma conditions, $\sigma$ is close to zero for $\alpha$ of 40° and above. This suggests that the growth of films at such oblique angles is dominated by oblique angle atomic impacts resulting in a columnar microstructure with low residual stress.[16]

As shown in Fig. 3(c), high hardness values ($H_M$ = 38 GPa) are measured in coatings from both runs for the $\alpha = 0°$ tilt angle. For larger $\alpha$ films, $H_M$ values for 0 and 10% of Ne cases diverge. Films deposited with 10% of Ne have consistently higher $H_M$ values. The same trend is replicated by the $\alpha$ dependence of $E_Y$ shown in Fig. 3(d). Films deposited with a 10% of Ne are stiffer. This trend could be explained by examining the evolution of film density shown in Fig. 3(e). It reveals that films deposited with the Ne-containing plasma have higher density .—although their their normalized deposition rates are largely the same [Fig. 3(a)]. This suggests that the deposition with a Ne-containing plasma is characterized by an increased target sputtering rate. Films deposited with a 100% Ar plasma have a density of 2.4 g/cm$^3$ at $\alpha = 0°$, $\sim$ 2.0 g/cm$^3$ for $\alpha$ in the range of $0 - 60°$, and 1.8 g/cm$^{-3}$ for $\alpha = 80°$. Films deposited with a 10% Ne mix exhibit a similar trend but with overall higher density values. Overall, the density in films is shown to be weakly dependent on substrate tilt angle, and this is especially the case for the 10% Ne samples. This behavior could be attributed to a larger ion-to-atom fraction and more efficient ion bombardment of the growing film surface for the case of Ne-containing plasma although additional systematic studies involving plasma diagnostics are currently needed to better understand film growth mechanisms and optimize the deposition process.

## IV. SUMMARY

We have used magnetron sputtering to deposit $B_4C$ films with an FFE source modified for direct cooling with the HiPIMS plasma discharge mode with two different working gases (pure Ar and an Ar-Ne mix with 10% of Ne) and substrates biased at $-25$ V. Higher plasma densities, as indicated by larger target and substrate currents, can be achieved by using larger process pressure and adding Ne to the working gas mixture. This work has

demonstrated that the density and mechanical properties of $B_4C$ films can be improved with the deposition in the HiPIMS mode in an Ar-Ne working gas mix. Our results demonstrate that the HiPIMS discharge mode coupled with Ar-Ne gas mixture expands the flexibility of magnetron sputter deposition of $B_4C$ and offers additional process control. However, it also increases process complexity, and more work is currently needed to better understand the physics of the HiPIMS $B_4C$ mixed plasma discharge with an FFE magnetron source.

## V. ACKNOWLEDGMENTS

This work was performed under the auspices of the U.S. DOE by LLNL under Contract DE-AC52-07NA27344.

## VI. DATA AVAILABILITY STATEMENT

The data that supports the findings of this study is available within the article.

## VII. AUTHOR DECLARATIONS

### A. Conflict of Interest

The authors have no conflicts to disclose.

## REFERENCES


[1]F. Thévenot, "Boron carbide—A comprehensive review," *Journal of the European Ceramic Society*, vol. 6, no. 4, pp. 205, 1990.

[2]S. G. Savio, et al., "An experimental study on ballistic performance of boron carbide tiles," *International Journal of Impact Engineering*, vol. 38, no. 7, pp. 535, 2011.

[3]S. Bhatia, et al., "A review on mechanical and tribological characterization of boron carbide reinforced epoxy composite," *Advanced Composite Materials*, vol. 30, no. 4, pp. 307, Taylor & Francis, 2021.

[4]B. S. Gajjar, et al., "Boron Carbide as High-Energy Radiation Shielding Material for ITER," *IEEE Transactions on Plasma Science*, vol. 50, no. 12, pp. 5078, 2022.

[5]Y. Q. Chen and B. H. Yan, "The technology of shielding design for nuclear reactor: A review," *Progress in Nuclear Energy*, vol. 161, 104741, 2023.

[6]S. W. Haan, et al., "Design and modeling of ignition targets for the National Ignition Facility," Physics of Plasmas, vol. 2, no. 6, pp. 2480, 1995.

[7]T. R. Dittrich, S. W. Haan, S. Pollaine, A. K. Burnham, and G. L. Strobel, "NIF capsule design update," Fusion Sci. Tech. **31**, 402 (1997).

[8]S. O. Kucheyev, et al., "Development of New Magnetron Sputter Deposition Processes for Laser Target Fabrication," *Fusion Science and Technology*, vol. 79, no. 7, pp. 823, American Nuclear Society, 2023.

[9]W. D. Westwood, Sputter deposition, AVS, New York (2003).

[10]A. K. Burnham, C. S. Alford, D. M. Makowiecki, T. R. Dittrich, R. J. Wallace, E. C. Honea, and C. M. King, "Evaluation of B4C as an Ablator Material for NIF Capsules," Fusion Sci. Tech. **31**, 456 (1997).

[11]J. B. Merlo, et al., "Magnetron sputter deposition of ultrathick boron carbide coatings on spherical substrates for inertial confinement fusion," *Surface and Coatings Technology*, vol. 477, 130321, 2024.130321.

[12]A. M. Engwall, L. B. Bayu Aji, S. Shin, P. B. Mirkarimi, J. H. Bae, and S. O. Kucheyev, J. Appl. Phys. **128**, 175301 (2020).

[13]L. B. Bayu Aji, et al., "Radio-frequency magnetron sputter deposition of ultrathick boron carbide films," *Journal of Vacuum Science & Technology A*, vol. 41, no. 2, 023407, 2023.

[14]L. B. Bayu Aji, et al., "Effect of substrate temperature on sputter-deposited boron carbide films," *Journal of Applied Physics*, vol. 131, no. 7, 075304, 2022.

[15]S. J. Shin, L. B. Bayu Aji, A. M. Engwall, J. H. Bae, G. V. Taylor, P. B. Mirkarimi, C. Aracne-Ruddle, J. Nguyen, C. W. N. Kong, and S. O. Kucheyev, Fusion Sci. Technol. **79**, 841 (2023).

[16]S. J. Shin, et al., "Oblique angle deposition of boron carbide films by magnetron sputtering," *Journal of Applied Physics*, vol. 130, no. 12, 125305, 2021.

[17]G. V. Taylor, et al., "Boron carbide films with reduced nodular defect density deposited by full-face erosion radio-frequency magnetron sputtering," *Journal of Vacuum Science & Technology A*, vol. 42, no. 4, 040401, 2024.

[18]S. J. Shin, et al., "Magnetron sputter deposition of boron carbide in Ne and Ar plasmas," *Journal of Applied Physics*, vol. 135, no. 8, 085303, 2024.

[19]V. Kouznetsov, K. Macak, J. M. Schneider, U. Helmersson, and I. Petrov, "A novel pulsed magnetron sputter technique utilizing very high target power densities," Surf. Coat. Technol. **122**, 290 (1999).

[20]J. T. Gudmundsson, N. Brenning, D. Lundin, and U. Helmersson, "High power impulse magnetron sputtering discharge," J. Vac. Sci. Technol. A **30**, 030801 (2012).

[21]S. Schmidt, et al., "Low-temperature growth of boron carbide coatings by direct current magnetron sputtering and high-power impulse magnetron sputtering," *Journal of Materials Science*, vol. 51, no. 23, pp. 10418, 2016.

[22]A. Aijaz, K. Sarakinos, D. Lundin, N. Brenning, and U. Helmersson, "A strategy for increased carbon ionization in magnetron sputtering discharges," Diamond and Related Materials **23**, 1 (2012).

[23]F. Haase, D. Lundin, S. Bornholdt, and H. Kersten, "On the Impact of Electron Temperature in Magnetron Sputtering Benchmarked with Energy Flux Measurements," Contrib. Plasma Phys. **55**, 701 (2015).

[24]W. C. Oliver and G. M. Pharr. "An improved technique for determining hardness and elastic modulus using load and displacement sensing indentation experiments." J. Mater. Res. 7, 1564 (1992).

[25]S. O. Kucheyev, A. V. Hamza, J. H. Satcher Jr, and M. A. Worsley. "Depth-sensing indentation of low-density brittle nanoporous solids." Acta Mater. 57, 3472 (2009).

[26]S. M. Rossnagel and H. R. Kaufman, "Current–voltage relations in magnetrons," *Journal of Vacuum Science & Technology A*, vol. 6, no. 2, pp. 223, 1988.

[27]I. Petrov, et al., "Comparison of Some Basic Plasma Parameters and Discharge Characteristics of Planar Magnetron Sputtering Discharges in Argon and Neon," *Contributions to Plasma Physics*, vol. 30, no. 2, pp. 223, 1990.

[28]S. J. Shin, J. H. Bae, A. M. Engwall, L. B. Bayu Aji, A. A. Baker, G. V. Taylor, J. B. Merlo, L. R. Sohngen, J. D. Moody, S. O. Kucheyev, Deoposition of ultrathick heavy-metal alloys on rotating substrates by high-power impulse magnetron sputtering: Target erosion effects, J. Appl. Phys. **135**, 035301 (2024).

TABLE I. Conditions and resulting film thicknesses of the two deposition runs of the present study. The substrate tilt angle ($\alpha$) is defined in the text.

| Parameter | Run 1 | Run 2 |
|---|---|---|
| Ne content in Ar-Ne mix (%) | 0 | 10 |
| Peak voltage (V) | 680 | 680 |
| Average power (W) | 210 | 370 |
| Peak target current (A) | 25 | 46 |
| Pulse frequency (Hz) | 50 | 50 |
| Pulse width ($\mu$s) | 500 | 500 |
| Substrate bias (V) | $-25$ | $-25$ |
| Pressure (mTorr) | 45 | 45 |
| Deposition time (h) | 3 | 3 |
| Target-to-substrate distance (mm) | 50 | 50 |
| Film thickness for $\alpha = 0^\circ$ ($\mu$m) | 2.8 | 4.6 |

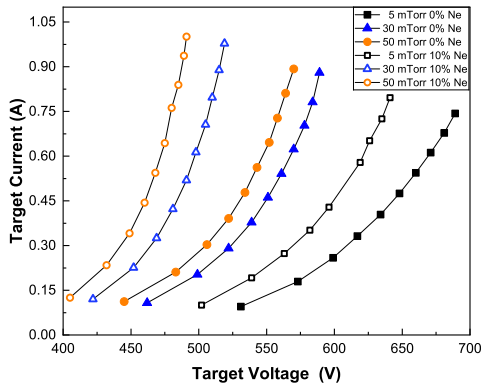


FIG. 1. Dependence of target current on the absolute value of (negative) target voltage for the DCMS discharge in Ar-Ne mixtures with 0 and 10% of Ne at 5, 30, and 50 mTorr, as indicated in the legend.

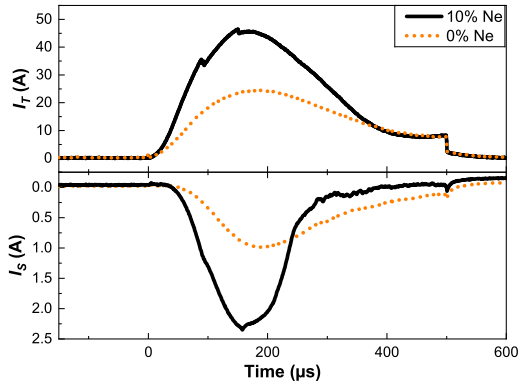


FIG. 2. Waveforms of (a) target current ($I_t$) and (b) substrate current ($I_s$) for Ar-Ne mixtures with 0 and 10% of Ne at 45 mTorr, a peak target voltage of 680 V, and a substrate bias of $-25$ V. Current of ions from the plasma is shown as positive in both panels. The legend in (a) applies to both panels.

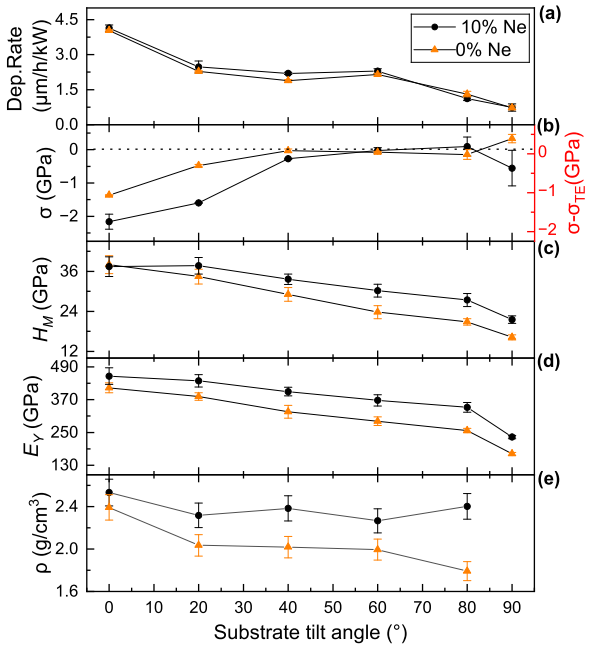


FIG. 3. Substrate tilt dependencies of (a) the deposition rate normalized to the average discharge power, (b) residual stress ($\sigma$, where $\sigma_{TE}$ is the stress contribution due to the thermal expansion mismatch between the substrate and the film), (c) Meyer's Hardness ($H_M$), (d) Young's Modulus ($E_Y$), and (e) mass density ($\rho$) of $B_4C$ films deposited at 45 mTorr in Ar-Ne mixtures with 0 and 10% of Ne, as indicated in the legend in (b), which applies to all five panels.